



# CHORUS

This is the accepted manuscript made available via CHORUS. The article has been published as:

## Focused thermal emission from a nanostructured SiC surface

Hamidreza Chalabi, Andrea Alù, and Mark L. Brongersma  
Phys. Rev. B **94**, 094307 — Published 23 September 2016

DOI: [10.1103/PhysRevB.94.094307](https://doi.org/10.1103/PhysRevB.94.094307)

# Focused thermal emission from a nanostructured SiC surface

Hamidreza Chalabi,<sup>1,2,\*</sup> Andrea Alù,<sup>2,†</sup> and Mark L. Brongersma<sup>1,‡</sup>

<sup>1</sup>*Geballe Laboratory for Advanced Materials, Stanford University, Stanford, California 94305, USA*

<sup>2</sup>*Department of Electrical and Computer Engineering,  
The University of Texas at Austin, Austin, Texas 78712, USA*

(Dated: September 7, 2016)

Incandescent sources that produce light from electrically-heated filaments or films tend to feature low efficiencies and offer poor spectral and angular control. We demonstrate that a judicious nanostructuring of a SiC surface can focus thermal emission of a preselected spectral range to a well-defined height above the surface. SiC is known to support electromagnetic surface waves that afford the required thermal emission control. Here, we provide general design rules for this type of focusing element that can be extended to other material systems, such as metals supporting surface plasmon-polariton waves. These rules are verified using full-wave calculations of the spatial variation of thermal emission. The obtained results can be regarded as the first steps toward developing more complex algorithms for the design of complex thermal lenses.

## INTRODUCTION

Thermal emitters have been the very first sources of light developed by humans. In spite of their long history, these light sources suffer from a number of limitations. These include the lack of proper control over the directionality and spatial localization, as well as the spectral and polarization properties of the emitted light. To overcome these limitations, efforts have been made to increase their spectral selectivity<sup>1–8</sup>, directionality<sup>9–14</sup>, or both<sup>15–17</sup>. Here, we demonstrate the ability to direct thermal radiation from a heated film of silicon carbide (SiC) to a small focus above its surface by judiciously nanopatterning the film. The ability to concentrate thermal radiation can impact the design and operation of next-generation thermo-photovoltaic cells<sup>18–21</sup>, afford control over local heat generation<sup>22–25</sup>, and it can mitigate challenges associated with thermal management in low thermal budget devices<sup>26,27</sup>.

Despite the superficial similarity to ordinary lenses, the design of the proposed lens for thermal radiation faces many additional challenges. Most notably, a conventional lens is illuminated by an external source, while the considered optical component serves as both the lens and the source of emission. When a conventional lens is illuminated by a monochromatic plane wave, the wave front is well-defined and can be shaped through refraction. In contrast, in a thermal lens the emission originates from thermal current sources everywhere within the lens material and their correlation is governed by the fluctuation dissipation theorem<sup>28,29</sup>. The pioneering work by Greffet<sup>10</sup> showed that directional emission can be achieved by decoupling thermally excited surface phonon polaritons (SPhPs) supported on a silicon carbide substrate. In this way, unity emissivity is obtained for a specific direction by using of corrugations on the surface of a planar SiC film, which would otherwise be highly reflective<sup>30</sup> (giving rise to a very low absorptance and emittance) in the mid-infrared spectral range. The supported surface waves in these structures make it possi-

ble to boost the spatial coherence length of the thermally excited electromagnetic fields<sup>31,32</sup>. A generalization of that work has also been explored by using coupled resonant cavities to overcome the spatial coherence length limitation that exists in the case of shallow gratings<sup>9</sup>. More advanced designs, such as bull’s eye structures patterned into metallic films, have also been considered in the literature for the purpose of beaming the thermal emission<sup>12,14</sup>. Moreover, further enhancement in thermal emission control by selective heating of nanostructures has been investigated recently<sup>33,34</sup>.

Here, we show how nanopatterning of SiC can enable focusing of thermal emission. While the nanopatterned scatterers on the surface may be considered isotropic emitters, the excitation of surface waves with a sufficiently long propagation length can be used to link the phases of the emission scattered by the nanostructures. Scatterers with appropriate size and position can then be used to direct decoupled waves in a desired fashion. Here, we present a design strategy for such lenses to augment the design of the metasurface optical components<sup>35–40</sup>. We start by demonstrating a lens with a focal length of  $50\mu\text{m}$  at a target wavelength of  $11.36\mu\text{m}$ . The thermal emission profile of this lens at its focal plane has a peak value around two and a half times larger than the asymptotic value, corresponding to the thermal emission of a smooth substrate, in a spot size of about  $10\mu\text{m}$ . The bandwidth of operation is relatively small due to the significant chromatic aberration<sup>40</sup> of the proposed lens design. We also demonstrate a similar lens at the same target wavelength with a focal length of  $100\mu\text{m}$  and a spot size of about  $20\mu\text{m}$ . The obtained design rules can be used for any desired focal length and operational frequency.

## THERMAL LENS OPERATION

Advances in gradient metasurfaces have enabled the realization of ultrathin optical elements capable of steering light<sup>35–40</sup>. These elements are constructed from a

dense array of optical antennas placed on a surface that can scatter light with a well-defined phase and amplitude. By controlling the phase of the scattered light at each location, the wave front can be manipulated, at will. Controlling thermal emission presents significant more challenges than conventional optical radiation. Figure 1a shows conceptually how a pattern of nanoscale antennas can direct thermal emission to a focus point above the surface for the case of thermal lenses. Here, we need to scatter thermally generated surface waves towards a focus by using of corrugations as scattering elements. To enable focusing, the size, shape, and spacing of the scattering elements on the surface need to be carefully chosen to obtain constructive interference of the scattered waves at a focal point of interest. To illustrate our approach to achieve this effect, we describe how a series of SiC beams can be placed on a smooth SiC surface to cause the decoupling and subsequent concentration of thermal radiation into a line-focus. To this end, we capitalize on the fact that thermally-driven currents near the surface of a SiC film effectively and preferentially couple to SPhPs rather than to free-space radiation. As such, the challenge of focusing thermal radiation can be rewritten as the one of appropriately decoupling SPhPs propagating towards the left and right directions along the surface. Figure 1b shows a simplified version of a thermal lens, composed of only three scatterers and a SPhP incident from the left. These scatterers need to be positioned in such a way that decoupled waves constructively interfere at a focal point above the surface. Since the structure is assumed to be mirror symmetric, considering a SPhP propagating in the opposite direction will lead to the same final requirements.

In order to achieve focusing, the phase pickup along paths 1, 2 and 3 needs to be close to each other. These phase pickups can be calculated through the knowledge of the SPhP dispersion relation. For the initial design, we use the simplifying assumption that the additional phase pickup caused by nanobeam decoupling is the same for all of the beams.

The phase difference between these three pathways can be calculated straightforwardly. Using the geometrical parameters defined in Fig. 1b, we have:

$$\theta_1 \doteq \phi_1 - \phi_2 = k_0 \left( \sqrt{d^2 + f^2} - f \right) - \Re[k_{SPhP}] d \quad (1)$$

$$\theta_2 \doteq \phi_3 - \phi_2 = k_0 \left( \sqrt{d^2 + f^2} - f \right) + \Re[k_{SPhP}] d \quad (2)$$

$$\theta_3 \doteq \phi_3 - \phi_1 = 2\Re[k_{SPhP}] d \quad (3)$$

In these equations,  $\phi_1$ ,  $\phi_2$ , and  $\phi_3$  represent the phases accumulated along the first, second, and third path, respectively, and  $\theta_1$ ,  $\theta_2$ , and  $\theta_3$  are defined as the phase difference between them. Moreover,  $k_0$  is the free-space

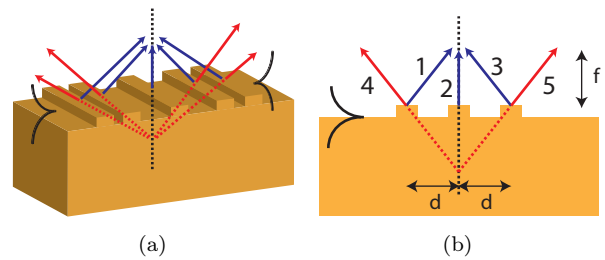


Figure 1: (a) Operation of a SiC thermal lens capable of focusing thermally generated surface waves (black) by decoupling them from appropriately positioned nanobeams to achieve constructive interference in a line-focus above the surface (blue arrows). The proposed design will lead to the generation of diverging waves at the same time (red arrows). (b) Scattering of a surface phonon polariton propagating to the right (black) by a simplified version of a thermal lens made of only three subwavelength beams. The arrows depict various pathways by which the surface wave can be decoupled to the far-field. Geometrical parameters are defined in this cross-sectional view of the structure.

wave vector at the frequency of interest and  $k_{SPhP}$  is the wave vector of the supported surface phonon polaritons. For our current study which considers beams with small heights, referred as shallow beams, we can safely assume that<sup>41</sup>  $k_{SPhP} = k_0 \sqrt{\epsilon_{SiC} / (1 + \epsilon_{SiC})}$ .

Note that these phases are wrapped, in radians, to the  $-\pi$  to  $\pi$  interval. In order to have constructive interference between these scattered waves, the absolute value of these phase differences between different paths should be as small as possible. At angular frequency  $\omega = 1.66 \times 10^{14} rad/s$ , as a sample frequency at which a SiC surface can support surface waves, these three phase differences can be calculated as a function of the spacing between neighboring beams  $d$ , as shown in Fig. 2. In this figure, the phase difference variation is calculated for two different focal lengths. Fig. 2a shows the phase variation for the case of  $f = 50 \mu m$ , while Fig. 2b corresponds to the case of  $f = 100 \mu m$ .

There are some ranges of distance  $d$  for which the absolute values of the phase differences are all smaller than  $\pi/2$ . These regions are shaded in Fig. 2. If the two side scatterers are positioned symmetrically relative to the central one at distances corresponding to the shaded regions, we expect them to effectively contribute to constructive interference in the desired focal point.

In addition to the focusing at the focal height of interest, fulfillment of the phase differences to be smaller than  $\pi/2$  leads at the same time to the generation of diverging waves. In fact, it can easily be verified that three scattered waves numbered as 4, 2, and 5 in Fig. 1b, can be thought of as diverging waves from a virtual source below the surface. Assuming that height of the beams is much smaller than the focal length, this imaginary source

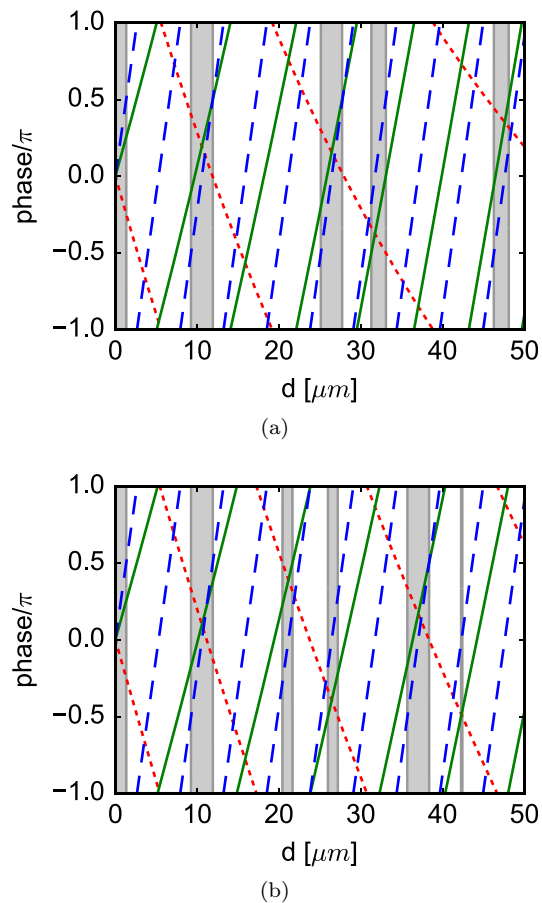


Figure 2: Phase difference between the waves scattered by SiC beams at the focal point as a function of the beam spacing  $d$ , for a focal length of (a)  $f = 50\mu\text{m}$  and (b)  $f = 100\mu\text{m}$ . In these figures, the red dotted lines show the variation of phase  $\theta_1$ , green solid lines show the variation of phase  $\theta_2$ , and blue dashed lines show the variation of the phase  $\theta_3$ . Shaded regions show ranges of distance  $d$  for which the absolute values of all the phase differences are smaller than  $\pi/2$ .

is positioned at the same distance from the surface as the focal point but is located inside the substrate.

Focusing can be enhanced by adding two more side scatterers, positioned symmetrically relative to the central beam at any appropriately chosen distance within the shaded regions in Fig. 2. This is because the scattered wave from the central beam has a phase difference smaller than  $\pi/2$  relative to scattered waves from the new side scatterers, as well as all the previous ones at the focal point of interest. This enables us to further enhance our thermal lenses by incorporating more scatterers symmetrically positioned at appropriate distances. This enhancement applies also to the generation of diverging waves (See Fig. 1a).

The above analysis provides us a straightforward design rule and also relevant physical insights on how to achieve and enhance thermal emission focusing. How-

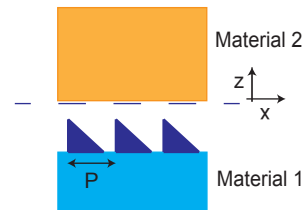


Figure 3: Schematic of the geometry used to perform thermal emission calculations. The thermal emission from an arbitrarily shaped periodic structure can be calculated at a specific height by placing a hypothetical planar body with a small loss at the height of interest and by looking at the thermal transfer between the periodic structure and this planar body.

ever, for the purpose of numerical assessment of the designed thermal lens, we need a method to rigorously calculate the lateral variation of thermal emission at the heights of interest. The following section presents such a method.

## ANALYTICAL FORMULATION

The thermal emission from an arbitrary object can be calculated considering the thermally-driven fluctuating currents inside the object. There are already some calculations in this regard available in the literature<sup>42</sup>. Here, we leverage our previous works on thermal transfer calculations<sup>43,44</sup> to obtain an expression for the thermal emission pointing outward from the nanostructure at different heights from its surface. The presented analysis is valid for periodic structures. However, for the case of non-periodic structures as in the current study, the same method can be used at the expense of choosing a fictitious periodicity large enough in order to remove the effect of adjacent blocks at the height of interest. We explored whether the chosen periodicity is large enough by quantifying the magnitude of thermal emission at the periodic boundaries at the height of interest, and comparing it with the thermal emission from the same material but with a flat surface. Furthermore, by considering increasing values of the periodicity we made sure the results are converged and there are no artifacts stemming from the periodicity.

In order to calculate the thermal emission of an arbitrarily shaped periodic structure at a specific height, we can place a hypothetical planar body with a small loss at the height of interest and look at the thermal transfer between the periodic structure and the planar body. By taking the limit of loss going to zero, we obtain the thermal emission of the periodic structure at this height. This provides a way to calculate the thermal emission at the height of interest based on the method that has already been developed for thermal transfer calculations between an arbitrarily shaped periodic structure and a

planar substrate<sup>43</sup>. However, the final result can be further simplified by analytically taking the limit of zero loss in the hypothetical planar body.

For the general case of periodic structures (See Fig. 3), we can express the electromagnetic Green functions, representing the electromagnetic response of the system to electric dipoles, in terms of the response of the system to plane waves by using the modified version of Sipe's formalism<sup>43,45</sup>. We assumed the  $z$  direction to be toward the planar body and normal to its plane. The convention used for the  $x$  direction is also shown in Fig. 3, and the plane  $z = 0$  is chosen as the position on which the thermal emission is calculated.

Following the notations used in<sup>43</sup>, we define  $\overrightarrow{G_E^a}(\omega, x, y, z, k_x, k_y)$  and  $\overrightarrow{G_H^a}(\omega, x, y, z, k_x, k_y)$  as:

$$\overrightarrow{G_E^a}(\omega, x, y, z, k_x, k_y) \triangleq \frac{-\omega\mu_0}{2k_z} \overrightarrow{G_{E,N}^a}(\omega, x, y, z, k_x, k_y) \quad (4)$$

$$\overrightarrow{G_H^a}(\omega, x, y, z, k_x, k_y) \triangleq \frac{-\omega}{2k_z c} \overrightarrow{G_{H,N}^a}(\omega, x, y, z, k_x, k_y) \quad (5)$$

where dimensionless quantities  $\overrightarrow{G_{E,N}^a}(\omega, x, y, z, k_x, k_y)$  and  $\overrightarrow{G_{H,N}^a}(\omega, x, y, z, k_x, k_y)$  are defined as:

$$\begin{aligned} \overrightarrow{G_{E,N}^a}(\omega, x, y, z, k_x, k_y) \triangleq & \\ \sum_b \left( \overrightarrow{Res_E}(\omega, x, y, z, \beta\hat{\beta}, z' = 0, \hat{p}) \hat{p} \right. & \\ \left. + \overrightarrow{Res_E}(\omega, x, y, z, \beta\hat{\beta}, z' = 0, \hat{s}) \hat{s} \right)_{ba} \hat{e}_b & \quad (6) \end{aligned}$$

$$\begin{aligned} \overrightarrow{G_{H,N}^a}(\omega, x, y, z, k_x, k_y) \triangleq & \\ \sqrt{\frac{\mu_0}{\epsilon_0}} \sum_b \left( \overrightarrow{Res_H}(\omega, x, y, z, \beta\hat{\beta}, z' = 0, \hat{p}) \hat{p} \right. & \\ \left. + \overrightarrow{Res_H}(\omega, x, y, z, \beta\hat{\beta}, z' = 0, \hat{s}) \hat{s} \right)_{ba} \hat{e}_b & \quad (7) \end{aligned}$$

where  $\hat{e}_b$  is the unitary vector in the direction  $b$ , which takes on the unitary vectors in  $x$ ,  $y$ , and  $z$  directions in the summation.  $\overrightarrow{G_E^a}(\omega, x, y, z, k_x, k_y)$  and  $\overrightarrow{G_H^a}(\omega, x, y, z, k_x, k_y)$  are the electric and magnetic fields at position  $x$ ,  $y$ , and  $z$ , produced by the unity component  $a$  of a current density at  $z' = 0$ . Note that  $\overrightarrow{Res_E}(\omega, x, y, z, \beta\hat{\beta}, z', \hat{p})$  and  $\overrightarrow{Res_E}(\omega, x, y, z, \beta\hat{\beta}, z', \hat{s})$  are electric field responses at position  $x$ ,  $y$ ,  $z$  to p and s polarized incident plane waves with transverse wave-vector  $\beta\hat{\beta}$  and unity electric field amplitude at position  $z'$  and angular frequency  $\omega$ . Also,  $\overrightarrow{Res_H}(\omega, x, y, z, \beta\hat{\beta}, z', \hat{p})$  and  $\overrightarrow{Res_H}(\omega, x, y, z, \beta\hat{\beta}, z', \hat{s})$  are magnetic field responses at position  $x$ ,  $y$ ,  $z$  to p

and s polarized incident plane waves, again with transverse wave vector  $\beta\hat{\beta}$  and unity electric field amplitude at position  $z'$  and angular frequency  $\omega$ . These electromagnetic responses can be obtained through rigorous coupled wave analysis (RCWA)<sup>46,47</sup>. Consequently,  $\overrightarrow{G_{E,N}^a}(\omega, x, y, z, k_x, k_y)$  and  $\overrightarrow{G_{H,N}^a}(\omega, x, y, z, k_x, k_y)$  can be calculated directly from the RCWA method, as well.

From the obtained results in Ref.<sup>43</sup>, the thermal conductance can be expressed as:

$$\begin{aligned} S(x) = & \frac{1}{16\pi^3} \sum_a \int_{\omega=0}^{+\infty} d\omega \epsilon''(\omega) \left( e^{\hbar\omega/k_b T} - 1 \right)^{-2} \\ & \times \int_{k_y=-\infty}^{+\infty} \int_{k_x=-\infty}^{+\infty} dk_x dk_y \frac{e^{\hbar\omega/k_b T}}{\Im(k_z)} \frac{\hbar^2 \omega^5}{|k_z|^2 k_b T^2 c^3} \\ & \times \Re \left( \overrightarrow{G_{E,N}^a}(\omega, x, k_x, k_y) \times \overrightarrow{G_{H,N}^{a*}}(\omega, x, k_x, k_y) \right)_z \quad (8) \end{aligned}$$

Note that we have removed  $y = 0$  and  $z = 0$  in the arguments of  $G_{H,N}^a$ ,  $G_{E,N}^a$  for brevity.

However, if we assume that the permittivity of the planar body is given by  $1 + j\delta$  and  $\beta < \omega/c$ , then in the limit of small loss, the imaginary part of  $k_z$ ,  $\Im(k_z)$ , takes the form of:

$$\begin{aligned} \Im(k_z) = & \Im \left( \sqrt{\epsilon \frac{\omega^2}{c^2} - \beta^2} \right) = \Im \left( \sqrt{(1 + j\delta) \frac{\omega^2}{c^2} - \beta^2} \right) \\ & \rightarrow k_{z,R} \Im \left( 1 + \frac{j\delta}{2} \frac{\omega^2}{c^2 k_{z,R}^2} \right) = \frac{\delta \omega^2}{2c^2 k_{z,R}} \quad (9) \end{aligned}$$

in which  $k_{z,R}$  is defined as  $k_z$  in the limit of zero loss. The integral contribution that comes from  $k_x$  and  $k_y$  outside the light cone,  $\beta > \omega/c$ , becomes negligible in the limit of small loss as we expect. Therefore, we obtain the following result for  $S(x)$ :

$$\begin{aligned} S(x) = & \frac{1}{8\pi^3 c} \sum_a \int_{\omega=0}^{+\infty} d\omega \left( e^{\hbar\omega/k_b T} - 1 \right)^{-2} \\ & \times \int \int_{\sqrt{k_x^2 + k_y^2} < \omega/c} dk_x dk_y e^{\hbar\omega/k_b T} \frac{1}{k_z} \frac{\hbar^2 \omega^3}{k_b T^2} \\ & \times \Re \left( \overrightarrow{G_{E,N}^a}(\omega, x, k_x, k_y) \times \overrightarrow{G_{H,N}^{a*}}(\omega, x, k_x, k_y) \right)_z \quad (10) \end{aligned}$$

where, we have reverted to use  $k_z$  again instead of  $k_{z,R}$  for brevity.

From the above expression, we obtain the following expression for thermal emission:

$$\begin{aligned} I(x) = & \frac{1}{8\pi^3 c} \sum_a \int_{\omega=0}^{+\infty} d\omega \int \int_{\sqrt{k_x^2 + k_y^2} < \omega/c} dk_x dk_y \hbar \omega^2 k_z^{-1} \\ & \times \Re \left( \overrightarrow{G_{E,N}^a}(\omega, x, k_x, k_y) \times \overrightarrow{G_{H,N}^{a*}}(\omega, x, k_x, k_y) \right)_z \quad (11) \end{aligned}$$

The total thermal emission is the average of the above function across a period and is defined as:

$$I_{total} = \frac{1}{P} \int_{x=0}^P I(x) dx \quad (12)$$

Note that the SI unit of this quantity is  $W/m^2$ . It is possible to further simplify these equations, though. If we assume that the top of the periodic structure is located at  $z = -h$ , then:

$$\begin{aligned} \overrightarrow{G_{E,N}^a}(\omega, x, k_x, k_y) &= \overrightarrow{E_P} \hat{\rho}_a + \overrightarrow{E_S} \hat{s}_a \\ \overrightarrow{G_{H,N}^a}(\omega, x, k_x, k_y) &= \overrightarrow{H_P} \hat{\rho}_a + \overrightarrow{H_S} \hat{s}_a \end{aligned} \quad (13)$$

Using the orthogonality of s and p polarization directions, we can verify the following:

$$\begin{aligned} \sum_a \Re \left( \overrightarrow{G_{E,N}^a}(\omega, x, k_x, k_y) \times \overrightarrow{G_{H,N}^{a*}}(\omega, x, k_x, k_y) \right)_z \\ = \Re (E_{P,x} H_{P,y}^* - E_{P,y} H_{P,x}^* + E_{S,x} H_{S,y}^* - E_{S,y} H_{S,x}^*) \end{aligned} \quad (14)$$

where

$$\begin{aligned} E_{P,x} &= \hat{\rho}_x e^{jk_z h} - S_n R_{sp,n} e^{-jk_{z,n} h + 2jn\pi x/P} \\ &\quad - \frac{jk_{z,n}}{k_0} C_n R_{pp,n} e^{-jk_{z,n} h + 2jn\pi x/P} \\ E_{P,y} &= \hat{\rho}_y e^{jk_z h} + C_n R_{sp,n} e^{-jk_{z,n} h + 2jn\pi x/P} \\ &\quad - \frac{jk_{z,n}}{k_0} S_n R_{pp,n} e^{-jk_{z,n} h + 2jn\pi x/P} \\ E_{S,x} &= \hat{s}_x e^{jk_z h} - S_n R_{ss,n} e^{-jk_{z,n} h + 2jn\pi x/P} \\ &\quad - \frac{jk_{z,n}}{k_0} C_n R_{ps,n} e^{-jk_{z,n} h + 2jn\pi x/P} \\ E_{S,y} &= \hat{s}_y e^{jk_z h} + C_n R_{ss,n} e^{-jk_{z,n} h + 2jn\pi x/P} \\ &\quad - \frac{jk_{z,n}}{k_0} S_n R_{ps,n} e^{-jk_{z,n} h + 2jn\pi x/P} \\ H_{P,x} &= \hat{s}_x e^{jk_z h} - j S_n R_{pp,n} e^{-jk_{z,n} h + 2jn\pi x/P} \\ &\quad + \frac{k_{z,n}}{k_0} C_n R_{sp,n} e^{-jk_{z,n} h + 2jn\pi x/P} \\ H_{P,y} &= \hat{s}_y e^{jk_z h} + j C_n R_{pp,n} e^{-jk_{z,n} h + 2jn\pi x/P} \\ &\quad + \frac{k_{z,n}}{k_0} S_n R_{sp,n} e^{-jk_{z,n} h + 2jn\pi x/P} \\ H_{S,x} &= -\hat{\rho}_x e^{jk_z h} - j S_n R_{ps,n} e^{-jk_{z,n} h + 2jn\pi x/P} \\ &\quad + \frac{k_{z,n}}{k_0} C_n R_{ss,n} e^{-jk_{z,n} h + 2jn\pi x/P} \\ H_{S,y} &= -\hat{\rho}_y e^{jk_z h} + j C_n R_{ps,n} e^{-jk_{z,n} h + 2jn\pi x/P} \\ &\quad + \frac{k_{z,n}}{k_0} S_n R_{ss,n} e^{-jk_{z,n} h + 2jn\pi x/P} \end{aligned} \quad (15)$$

In these equations,  $R_{ss,n}$ ,  $R_{pp,n}$ ,  $R_{sp,n}$ , and  $R_{ps,n}$  are the co-polarization and cross polarization reflection coefficients of the s and p polarized incident waves. Moreover,  $k_{z,n}$  is the z component of the wave vector for the  $n$ th diffracted harmonic, and the summation over repeated index  $n$  is implied.

In addition, the following definitions are used:

$$\begin{aligned} C_n &= \frac{k_{x,n}}{\sqrt{k_y^2 + k_{x,n}^2}} \\ S_n &= \frac{k_y}{\sqrt{k_y^2 + k_{x,n}^2}} \end{aligned} \quad (16)$$

and

$$\begin{aligned} (\hat{\rho}_x \quad \hat{\rho}_y \quad \hat{\rho}_z) &= \frac{1}{k_0 \sqrt{k_x^2 + k_y^2}} (k_z k_x \quad k_z k_y \quad -k_x^2 - k_y^2) \\ (\hat{s}_x \quad \hat{s}_y \quad \hat{s}_z) &= \frac{1}{\sqrt{k_x^2 + k_y^2}} (-k_y \quad k_x \quad 0) \end{aligned} \quad (17)$$

Moreover:

$$\begin{aligned} k_{x,n} &= k_x + \frac{2\pi n}{P} \\ k_{z,n} &= \sqrt{\frac{\omega^2}{c^2} - k_{x,n}^2 - k_y^2} \end{aligned} \quad (18)$$

From the above relations, we can obtain an expression for the emission intensity variation with position. The necessary steps are a bit lengthy but straightforward. Here, we report the simplified expressions.

For this purpose we define  $D_n$  as

$$\begin{aligned} D_n &= \left( \frac{k_0}{k_z} (\hat{\rho}_x C_n + \hat{\rho}_y S_n) + \frac{k_{z,n}}{k_z} (\hat{s}_x S_n - \hat{s}_y C_n) \right) \\ &\quad \times (R_{ss,n} + j R_{pp,n}) \\ &\quad - \left( \frac{k_0}{k_z} (\hat{s}_x C_n + \hat{s}_y S_n) - \frac{k_{z,n}}{k_z} (\hat{\rho}_x S_n - \hat{\rho}_y C_n) \right) \\ &\quad \times (R_{sp,n} - j R_{ps,n}) \end{aligned} \quad (19)$$

and  $A_{n,m}$ ,  $B_{n,m}$ , and  $C_{n,m}$  as the following:

$$\begin{aligned} A_{n,m} &= \left( R_{ss,n} R_{ss,m}^* + R_{sp,n} R_{sp,m}^* + R_{pp,n} R_{pp,m}^* + \right. \\ &\quad \left. R_{ps,n} R_{ps,m}^* \right) (S_n S_m + C_n C_m) \frac{k_{z,n} + k_{z,m}^*}{2k_z} \end{aligned} \quad (20)$$

$$\begin{aligned} B_{n,m} &= \left( R_{pp,n} R_{sp,m}^* + R_{ss,n} R_{ps,m}^* + R_{sp,n} R_{pp,m}^* + \right. \\ &\quad \left. R_{ps,n} R_{ss,m}^* \right) (C_n S_m - S_n C_m) \frac{k_0^2 + k_{z,n} k_{z,m}^*}{2k_0 k_z} \end{aligned} \quad (21)$$

$$C_{n,m} = A_{n,m} + jB_{n,m} \quad (22)$$

It can be readily verified that  $D_0 = 0$ . After simplification, we obtain that:

$$\begin{aligned} & \Re \left\{ E_{P,x} H_{P,y}^* - E_{P,y} H_{P,x}^* + E_{S,x} H_{S,y}^* - E_{S,y} H_{S,x}^* \right\} \\ &= \frac{2k_z}{k_0} + \frac{k_z}{k_0} \sum_{n \neq 0} \Re \left( D_n e^{2jn\pi x/P} e^{-jk_z h - jk_{z,n} h} \right) \\ & - \frac{k_z}{k_0} \sum_{n,m} \Re \left( C_{n,m} e^{jk_{z,m}^* h - jk_{z,n} h} e^{2j(n-m)\pi x/P} \right) \quad (23) \end{aligned}$$

Therefore, we obtain the following equation expressing the thermal emission at position  $x$  and height  $h$ :

$$\begin{aligned} I(x) &= \frac{1}{8\pi^3} \sum_a \int_{\omega=0}^{+\infty} d\omega \hbar \omega \left( e^{\hbar\omega/k_b T} - 1 \right)^{-1} \\ & \int \int_{\sqrt{k_x^2 + k_y^2} < \omega/c} dk_x dk_y \left\{ 2 \right. \\ & - \sum_{n,m} \Re \left( C_{n,m} e^{jk_{z,m}^* h - jk_{z,n} h} e^{2j(n-m)\pi x/P} \right) \\ & \left. + \sum_{n \neq 0} \Re \left( D_n e^{2jn\pi x/P} e^{-jk_z h - jk_{z,n} h} \right) \right\} \quad (24) \end{aligned}$$

It is clear from the above equation that if we have the full vectors of reflection coefficients  $R_{ss}$ ,  $R_{pp}$ ,  $R_{sp}$ , and  $R_{ps}$ , we can calculate the normal component of the thermal emission at any point. These reflection coefficients can be obtained from a stable version of the RCWA technique with a highly improved convergence rate to save computational time<sup>48,49</sup>.

From the above equation and by using the fact that  $k_{z,n}$  is either purely imaginary or purely real, we have:

$$\begin{aligned} I_{total} &= \frac{1}{8\pi^3} \sum_a \int_{\omega=0}^{+\infty} d\omega \hbar \omega \left( e^{\hbar\omega/k_b T} - 1 \right)^{-1} \\ & \times \int \int_{\sqrt{k_x^2 + k_y^2} < \omega/c} dk_x dk_y \left\{ \right. \\ & 1 - \sum_n \frac{\Re(k_{z,n})}{k_z} (R_{sp,n} R_{sp,n}^* + R_{ss,n} R_{ss,n}^*) + \\ & \left. 1 - \sum_n \frac{\Re(k_{z,n})}{k_z} (R_{ps,n} R_{ps,n}^* + R_{pp,n} R_{pp,n}^*) \right\} \quad (25) \end{aligned}$$

This proves the independence of the total thermal emission on the height  $h$ , as expected. This last equation is in fact the famous equation for the gray body emission, which tells that the thermal emission of a gray body is the black body radiation modified by the corresponding emissivities for p and s polarizations. In fact,

the first two terms inside the curly bracket show the emissivity/absorption for s polarization and the second two terms show the emissivity/absorption for p polarization. We stress that the above results are obtained for the case of arbitrarily shaped periodic structures. In principle, it is possible to increase the periodicity to apply the method for arbitrarily shaped non periodic structures. However, this comes at the price of having to take into account a very large number of harmonics, which makes the calculations slower.

## NUMERICAL RESULTS

Using the exact method explained in the previous section, we calculated the lateral variation of thermal emission at angular frequency  $\omega = 1.66 \times 10^{14} rad/s$  from the structure shown in Fig. 1b for different beam spacings  $d$ . For these calculations, we have considered SiC beams with different heights and widths to serve as scatterers. In our numerical calculations, we assumed that the relative permittivity of SiC to be  $\epsilon = \epsilon_\infty + \omega_0^2 (\epsilon_s - \epsilon_\infty) (\omega_0^2 - \omega^2 + i\omega\delta)^{-1}$ , with  $\epsilon_\infty = 6.7$ ,  $\epsilon_s = 10$ ,  $\delta/\omega_0 = 0.006$  and  $\omega_0/(2\pi) = 2.38 \times 10^{13} sec^{-1} (12.6 \mu m)$ <sup>50,51</sup>. The temperature of the sample is taken to be  $T = 315K$  in these numerical calculations. The results of these calculations for different distances  $d$  are summarized in Fig. 4 for three different choices of width  $w$ , and height  $h$  of the beams. Figure 4a shows the variation of thermal emission at angular frequency  $\omega = 1.66 \times 10^{14} rad/s$  calculated at the focal height of  $f = 50 \mu m$  and Fig. 4b shows the corresponding variation for the focal height of  $f = 100 \mu m$ .

For each beam shape, we see oscillations in the magnitude of the thermal emission as a function of spacing. Large beams are more effective at decoupling the SPhPs from the surface and produce more thermal emission. However, the peak locations of thermal emission appears to be largely independent of the width and height of the beams. This indicates that the beams scatter light with a phase that is largely independent of the neighbors, in line with our previous assumptions. More interestingly, most of the peak locations are located inside the shaded regions in Fig. 2. There are two additional small peaks for the case of  $f = 50 \mu m$  in Fig. 4a, which correspond to the region in Fig. 2a that only one or two of the phase differences, rather than all three, are smaller than  $\pi/2$ .

It should be noted that in the phase calculation analysis of Fig. 2 none of the scattering properties of the individual beams is taken into consideration, and also the interaction between them is not considered. However, it can be seen that this analysis still provides significant insights about the optimal distances  $d$  that lead to a peak in thermal emission at the focal point. The heights of the beams are assumed to be  $250nm$  and  $400nm$  in the considered structures. These heights are chosen to be smaller than the penetration length of the supported SPhP in a planar SiC in order to satisfy the condition for shallow

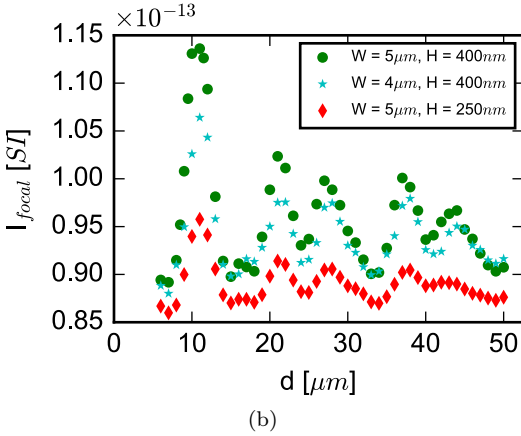
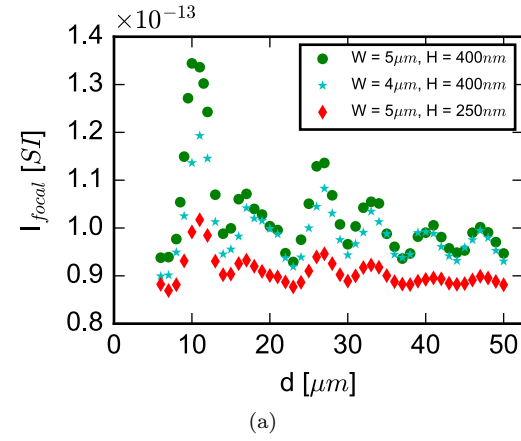


Figure 4: Thermal emission variation with the beam spacing  $d$ , at angular frequency  $\omega = 1.66 \times 10^{14} \text{rad/s}$  for the structure shown in Fig. 1b, at the focal height of (a)  $f = 50 \mu\text{m}$  and (b)  $f = 100 \mu\text{m}$ . These calculations are performed for three different choices of the width and height of the scattering nanobeams.

beams. It is expected that using of the beams with larger heights, will lead to a larger deviation of the dispersion of supported surface waves from the ones that are supported by a planar structure. For such large heights, we expect that the simple explanation of the peak location of thermal emission in terms of phase differences to become less valid, and the interactions of the beams with each other to become more important.

As it was pointed out earlier, by putting scatterers at distances corresponding to the peaks of thermal emission, we can further enhance the focusing effect. For this purpose, scatterers with height  $h = 400 \text{nm}$  and width  $w = 5 \mu\text{m}$  are used in the following calculations. Figure 5a shows the lateral and vertical variation of thermal emission at angular frequency  $\omega = 1.66 \times 10^{14} \text{rad/s}$  for a lens structure that is made of nine scatterers, with one of them positioned at the center and the others symmetrically positioned at distances  $d = 10 \mu\text{m}$ ,  $d = 27 \mu\text{m}$ ,  $d = 33 \mu\text{m}$ , and  $d = 47 \mu\text{m}$  from the center according to the peak locations of Fig. 4a. This figure clearly

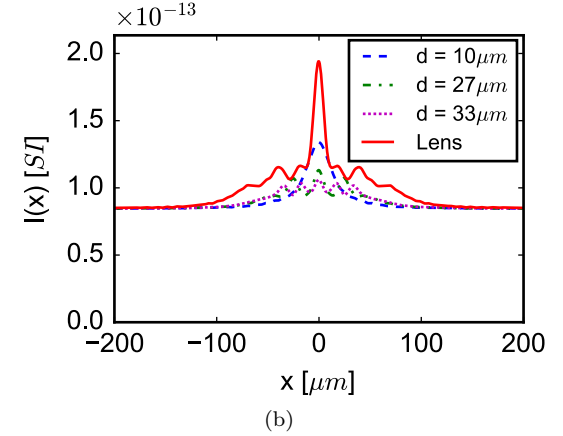
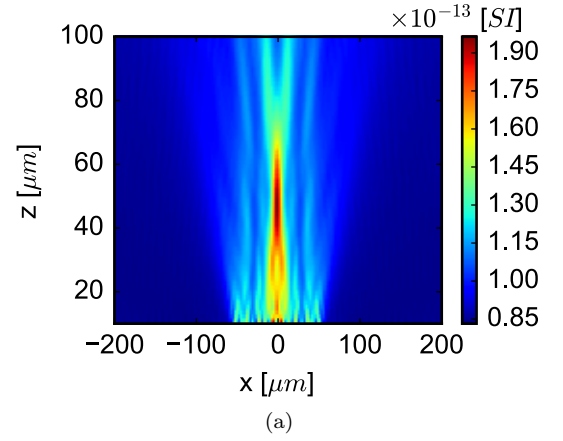


Figure 5: (a) Thermal emission lateral variation at different heights at angular frequency  $\omega = 1.66 \times 10^{14} \text{rad/s}$ . (b) Thermal emission lateral variation at the focal height of  $f = 50 \mu\text{m}$ . This variation is plotted along with the corresponding variations if only three scatterers were used with different beam spacings  $d$ .

illustrates the focusing of thermal emission at the expected focal height of  $f = 50 \mu\text{m}$ . The calculations are performed based on the exact method explained earlier, using 641 number of harmonics in order to achieve an accuracy of %5 for thermal emission calculations. A periodicity of  $400 \mu\text{m}$  is used for these calculations, in order to avoid interference effects of neighboring sites at the heights of interest. In addition, in order to speed up the calculations, the necessary integration tasks in  $k$  space are distributed among several computational units using MPI<sup>52</sup> for parallelization.

The lateral variation of thermal emission at angular frequency  $\omega = 1.66 \times 10^{14} \text{rad/s}$  at the designed focal height is also shown in Fig. 5b. This lateral variation is plotted along with the corresponding variations obtained if only three scatterers were used, as in Fig. 1b, with different beam spacings  $d$ . This figure clearly shows the value of adding more scatterers to enhance the thermal lens. We should reemphasize that the mechanism

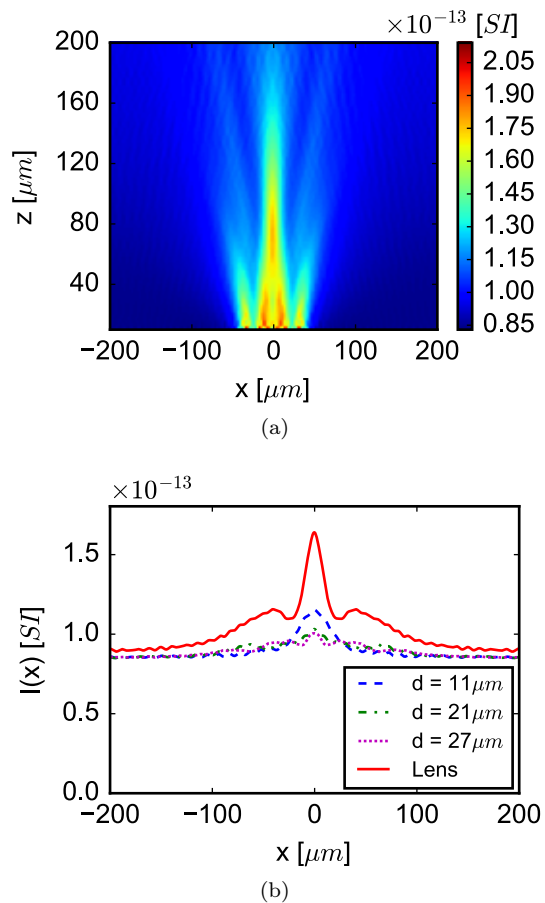


Figure 6: (a) Thermal emission lateral variation at different heights at angular frequency  $\omega = 1.66 \times 10^{14} \text{rad/s}$ . (b) Thermal emission lateral variation at the focal height of  $f = 100 \mu\text{m}$ . This variation is plotted along with the corresponding variations if only three scatterers were used with different beam spacings  $d$ .

of focusing presented here is based on decoupling surface waves which are only supported for p polarization. For the purpose of comparison, the black body radiation limit in the considered frequency and temperature is equal to  $2.47 \times 10^{-12} [ST]$ . As this figure shows, the designed thermal lens has a spot size of about  $10 \mu\text{m}$  and its emission peak value is about two and a half times larger than the asymptotic value. The asymptotic value, which is equal to the thermal emission of a flat substrate, can easily be calculated directly by considering the angular emissivity of a flat substrate at different spherical angles and integrating over all of them. The spot size of this thermal lens is similar to the diffraction limited spot size of ordinary lenses operating at the same wavelength. Moreover, the generation of a laterally confined spot size is similar to what has been observed in beaming light using plasmonic bull's eye antennas<sup>53</sup>.

Figure 6 also shows that a similar lens structure can be used to enhance thermal emission at angular frequency

$\omega = 1.66 \times 10^{14} \text{rad/s}$  at a focal point located at height of  $f = 100 \mu\text{m}$ . In this case again nine scatterers are used with one of them positioned at the center and the others symmetrically positioned at distances of  $d = 11 \mu\text{m}$ ,  $d = 21 \mu\text{m}$ ,  $d = 27 \mu\text{m}$ , and  $d = 37 \mu\text{m}$  from the center based on the peak locations obtained from Fig. 4b. As it is clear from Fig. 6b, this lens has a bit larger spot size compared to the previous one. This can be attributed to the decrease of the spatial coherence length as we move towards the far-field.

Even though the above calculations are performed for a specific frequency, similar calculations and designs can be performed for any other frequency, as long as a surface wave is supported in the considered material. Our additional calculations indicate that the above lens will somewhat focus also lower frequencies in the vicinity of its operational frequency to smaller focal heights, and vice versa. This is somehow similar to what is seen for Fresnel zone plates in which a lens designed for a specific frequency will also focus light at lower frequencies to shorter focal lengths and vice versa. The above mentioned results show that these lenses are able to increase the thermal emission at the focal point by about 2 to 3 times. Further enhancement of the thermal emission at the focal height can be achieved by increasing the number of scatterers as far as they are not located too far from the focal point and can effectively contribute to the enhancement. In addition, the size of the scatterers can be further optimized for this purpose. In Fig. 4 only three different sizes of scatterers are considered, and in the designed lenses all of the scatterers are assumed to be of the same size. These limitations can be removed in a more complex design routine. For instance, scatterers of different sizes may be considered in a practical design. Considering all of these possibilities will lead to a large parameter space for the purpose of optimization. However, calculation of the thermal emission for a specific structure can itself already be a relatively time consuming computational task. Because of that, using brute force analysis of variation of different defining geometrical parameters in order to optimize the lens structure seems impossible. In this sense, more creative and time efficient algorithms for further enhancement of these lenses are yet to be envisioned. We believe that the current design rule and calculation method can provide an insight and a roadmap toward such a purpose.

## CONCLUSIONS

In this article, we have considered the use of corrugations on top of a flat SiC substrate supporting surface waves at the interface with free-space, for the purpose of managing its thermal emission properties. The surface waves can be used to boost the spatial coherence length of the thermally excited electromagnetic fields. Scattering of these surface waves in periodic structures for emissivity enhancement at certain angles has been explored in

the literature. In spite of this, directly focusing thermal emission to a certain point in space has not been previously explored to a large extent. By considering a symmetric pattern of scatterers in a non periodic structure, we have studied the conditions for which such scatterers are able to enhance thermal emission at the focal height of interest. Moreover, we have investigated the thermal emission variation as a function of the distance between scatterers in a structure composed of three scatterers. Based on the obtained results, we have further enhanced the thermal emission focusing by using more scatterers. The explained design rules and techniques, applied here to a specific operational frequency of interest, can easily

be extended to other frequency ranges. We believe that the obtained results will provide the first building blocks in the search toward the design and realization of ideal thermal lenses.

## ACKNOWLEDGMENTS

This work was partially supported by the Office of Naval Research with grant No. N00014-15-1-2685 and a Grainger Foundation Frontiers of Engineering Grant.

- 
- \* [hr.chalabi@utexas.edu](mailto:hr.chalabi@utexas.edu)  
 † [alu@mail.utexas.edu](mailto:alu@mail.utexas.edu)  
 ‡ [brongersma@stanford.edu](mailto:brongersma@stanford.edu)
- <sup>1</sup> J. A. Schuller, T. Taubner, and M. L. Brongersma, *Nature Photonics* **3**, 658 (2009).
  - <sup>2</sup> H. T. Miyazaki, T. Kasaya, M. Iwanaga, B. Choi, Y. Sugimoto, and K. Sakoda, *Applied Physics Letters* **105**, 121107 (2014).
  - <sup>3</sup> X. Liu, T. Tyler, T. Starr, A. F. Starr, N. M. Jokerst, and W. J. Padilla, *Physical Review Letters* **107**, 045901 (2011).
  - <sup>4</sup> Y.-C. Chang, C.-M. Wang, M. N. Abbas, M.-H. Shih, and D. P. Tsai, *Optics Express* **17**, 13526 (2009).
  - <sup>5</sup> I. Puscasu and W. L. Schaich, *Applied Physics Letters* **92**, 233102 (2008).
  - <sup>6</sup> P. J. Hesketh, J. N. Zemel, and B. Gebhart, *Nature* **324**, 549 (1986).
  - <sup>7</sup> A. Battula and S. C. Chen, *Physical Review B* **74**, 245407 (2006).
  - <sup>8</sup> I. Celanovic, D. Perreault, and J. Kassakian, *Physical Review B* **72**, 075127 (2005).
  - <sup>9</sup> N. Dahan, A. Niv, G. Biener, Y. Gorodetski, V. Kleiner, and E. Hasman, *Physical Review B* **76**, 45427 (2007).
  - <sup>10</sup> J.-J. Greffet, R. Carminati, K. Joulain, J.-P. Mulet, S. Mainguy, and Y. Chen, *Nature* **416**, 61 (2002).
  - <sup>11</sup> M. Laroche, C. Arnold, F. Marquier, R. Carminati, J.-J. Greffet, S. Collin, N. Bardou, and J.-L. Pelouard, *Optics Letters* **30**, 2623 (2005).
  - <sup>12</sup> S. E. Han and D. J. Norris, *Optics express* **18**, 4829 (2010).
  - <sup>13</sup> C. Arnold, F. Marquier, M. Garin, F. Pardo, S. Collin, N. Bardou, J.-L. Pelouard, and J.-J. Greffet, *Physical Review B* **86**, 035316 (2012).
  - <sup>14</sup> J. H. Park, S. E. Han, P. Nagpal, and D. J. Norris, *ACS Photonics* **3**, 494 (2016).
  - <sup>15</sup> D. Costantini, A. Lefebvre, A.-L. Coutrot, I. Moldovan-Doyen, J.-P. Hugonin, S. Boutami, F. Marquier, H. Benisty, and J.-J. Greffet, *Physical Review Applied* **4**, 014023 (2015).
  - <sup>16</sup> M. Makhsiyani, P. Bouchon, J. Jaeck, J.-L. Pelouard, and R. Haïdar, *Applied Physics Letters* **107**, 251103 (2015).
  - <sup>17</sup> M. De Zoysa, T. Asano, K. Mochizuki, A. Oskooi, T. Inoue, and S. Noda, *Nature Photonics* **6**, 535 (2012).
  - <sup>18</sup> S. Y. Lin, J. Moreno, and J. G. Fleming, *Applied Physics Letters* **83**, 380 (2003).
  - <sup>19</sup> S. Fan, *Nature nanotechnology* **9**, 92 (2014).
  - <sup>20</sup> A. Lenert, D. M. Bierman, Y. Nam, W. R. Chan, I. Celanović, M. Soljačić, and E. N. Wang, *Nature Nanotechnology* **9**, 126 (2014).
  - <sup>21</sup> O. Ilic, P. Bermel, G. Chen, J. D. Joannopoulos, I. Celanovic, and M. Soljačić, *Nature Nanotechnology* (2016), 10.1038/nnano.2015.309.
  - <sup>22</sup> L. Cao, D. N. Barsic, A. R. Guichard, and M. L. Brongersma, *Nano Letters* **7**, 3523 (2007).
  - <sup>23</sup> J. R. Adleman, D. A. Boyd, D. G. Goodwin, and D. Psaltis, *Nano Letters* **9**, 4417 (2009).
  - <sup>24</sup> L. R. Hirsch, R. J. Stafford, J. A. Bankson, S. R. Sershen, B. Rivera, R. E. Price, J. D. Hazle, N. J. Halas, and J. L. West, *Proceedings of the National Academy of Sciences* **100**, 13549 (2003).
  - <sup>25</sup> B. F. Soares, F. Jonsson, and N. I. Zheludev, *Physical Review Letters* **98**, 153905 (2007).
  - <sup>26</sup> J. Cho and K. E. Goodson, *Nature Materials* **14**, 136 (2015).
  - <sup>27</sup> J. Schlee, J. Mateos, I. Íñiguez-de-la Torre, N. Wadefalk, P. A. Nilsson, J. Grahn, and A. J. Minnich, *Nature Materials* **14**, 187 (2014).
  - <sup>28</sup> W. Eckhardt, *Optics Communications* **41**, 305 (1982).
  - <sup>29</sup> K. Joulain, J.-P. Mulet, F. Marquier, R. Carminati, and J.-J. Greffet, *Surface Science Reports* **57**, 59 (2005), [arXiv:0504068 \[physics\]](https://arxiv.org/abs/0504068).
  - <sup>30</sup> F. Ghmari, T. Ghbara, M. Laroche, R. Carminati, and J.-J. Greffet, *Journal of Applied Physics* **96**, 2656 (2004).
  - <sup>31</sup> E. Wolf and D. F. V. James, *Reports on Progress in Physics* **59**, 771 (1996).
  - <sup>32</sup> R. Carminati and J.-J. Greffet, *Physical Review Letters* **82**, 1660 (1999).
  - <sup>33</sup> S. E. Han and D. J. Norris, *Physical Review Letters* **104**, 043901 (2010).
  - <sup>34</sup> W. Jin, A. G. Polimeridis, and A. W. Rodriguez, *Physical Review B* **93**, 121403 (2016).
  - <sup>35</sup> N. Yu, P. Genevet, M. A. Kats, F. Aieta, J.-P. Tetienne, F. Capasso, and Z. Gaburro, *Science* **334**, 333 (2011).
  - <sup>36</sup> N. Yu and F. Capasso, *Nature Materials* **13**, 139 (2014).
  - <sup>37</sup> F. Aieta, P. Genevet, M. A. Kats, N. Yu, R. Blanchard, Z. Gaburro, and F. Capasso, *Nano Letters* **12**, 4932 (2012).
  - <sup>38</sup> N. I. Zheludev and Y. S. Kivshar, *Nature Materials* **11**, 917 (2012).
  - <sup>39</sup> D. Lin, P. Fan, E. Hasman, and M. L. Brongersma, *Science* **345**, 298 (2014).

- <sup>40</sup> F. Aieta, M. A. Kats, P. Genevet, and F. Capasso, *Science* **347**, 1342 (2015).
- <sup>41</sup> H. Raether, *Surface plasmons on smooth surfaces* (Springer, 1988).
- <sup>42</sup> S. E. Han, *Physical Review B* **80**, 155108 (2009).
- <sup>43</sup> H. Chalabi, E. Hasman, and M. L. Brongersma, *Physical Review B* **91**, 14302 (2015).
- <sup>44</sup> H. Chalabi, E. Hasman, and M. L. Brongersma, *Physical Review B* **91**, 174304 (2015).
- <sup>45</sup> J. E. Sipe, *Journal of the Optical Society of America B* **4**, 481 (1987).
- <sup>46</sup> M. G. Moharam, E. B. Grann, D. A. Pommet, and T. K. Gaylord, *Journal of the Optical Society of America A* **12**, 1068 (1995).
- <sup>47</sup> M. G. Moharam, D. A. Pommet, E. B. Grann, and T. K. Gaylord, *Journal of the Optical Society of America A* **12**, 1077 (1995).
- <sup>48</sup> P. Lalanne and G. M. Morris, *Journal of the Optical Society of America A* **13**, 779 (1996).
- <sup>49</sup> L. Li, *Journal of the Optical Society of America A* **13**, 1870 (1996).
- <sup>50</sup> W. Spitzer, D. Kleinman, and D. Walsh, *Physical Review* **113**, 127 (1959).
- <sup>51</sup> W. Spitzer, D. Kleinman, and C. Frosch, *Physical Review* **113**, 133 (1959).
- <sup>52</sup> W. Gropp, E. Lusk, and A. Skjellum, *Using MPI: Portable parallel programming with the message-passing interface* (MIT Press, Cambridge, Mass, 1999).
- <sup>53</sup> H. J. Lezec, A. Degiron, E. Devaux, R. A. Linke, L. Martin-Moreno, F. J. Garcia-Vidal, and T. W. Ebbesen, *Science (New York, N.Y.)* **297**, 820 (2002).